Magnetowetting and Sliding Motion of a Sessile Ferrofluid Droplet in the Presence of a Permanent Magnet

ARTICLE *in* LANGMUIR · AUGUST 2010

Impact Factor: 4.46 · DOI: 10.1021/la101474e · Source: PubMed

5 AUTHORS, INCLUDING:

Nam-Trung Nguyen
Griffith University
344 PUBLICATIONS **5,983** CITATIONS

SEE PROFILE

Guiping Zhu
Nanyang Technological University
7 PUBLICATIONS **70** CITATIONS

SEE PROFILE

Say hwa Tan
Griffith University
29 PUBLICATIONS **407** CITATIONS

SEE PROFILE

Langmuir Article

pubs.acs.org/Langmuir

Magnetowetting and Sliding Motion of a Sessile Ferrofluid Droplet in the Presence of a Permanent Magnet

Nam-Trung Nguyen,* Guiping Zhu, Yong-Chin Chua, Vinh-Nguyen Phan, and Say-Hwa Tan

School of Mechanical and Aerospace Engineering, Nanyang Technological University, 50 Nanyang Avenue, Singapore, Singapore 639798

Received April 14, 2010. Revised Manuscript Received June 18, 2010

Motion of a droplet on a planar surface has applications in droplet-based lab on a chip technology. This paper reports the experimental results of the shape, contact angles, and motion of ferrofluid droplets driven by a permanent magnet on a planar homogeneous surface. The water-based ferrofluid in use is a colloidal suspension of single-domain magnetic nanoparticles. The effect of the magnetic field on the apparent contact angle of the ferrofluid droplet was first investigated. The results show that an increasing magnetic flux decreases the apparent contact angle of a sessile ferrofluid droplet. Next, the dynamic contact angle was investigated by observing the shape and the motion of a sessile ferrofluid droplet. The advancing and receding contact angles of the moving ferrofluid were measured at different moving speeds and magnetic field strengths. The measured contact angles were used to estimate the magnitude of the forces involved in the sliding motion. Scaling analysis was carried out to derive the critical velocity, beyond which the droplet is not able to catch up with the moving magnet.

Introduction

Controlled actuation of liquid droplets on a planar surface is an important task in droplet-based microfluidics. A droplet can work as a vehicle for transporting reagents. The confined space in a droplet represents an ideal reactor for many chemical and biochemical processes. A planar surface allows the implementation of two-dimensional droplet-based microfluidic systems which can handle droplets individually. Droplets on a planar surface have higher flexibility than those confined in a microchannel. Actuation of droplets on a planar surface can be achieved by different means: surface energy gradient,[1] thermal gradient,[2] electrowetting,[3] surface acoustic waves,[4] vibration,[5] and magnetism. Recently, Genzer and Bhat[6] gave a review on the fabrication of surfaces with gradient structures. Mogenthaler et al.[7] reviews the different methods for fabricating surface gradients of chemistry an morphology. These surface gradients allow the transport of sessile droplets without external energy. Self-running droplets on surface gradients have been reported by a number of research groups.[8−10] Sliding motion of sessile droplets on super hydrophobic surfaces has also been extensively investigated. The droplet was driven by gravity[11] or in the presence of an electric field.[12,13] Bormashenko reported preliminary results on using a magnet to drive marbles and droplets containing ferrofluid.[14] To the best of our knowledge, no detailed work has been reported on the effect of a magnetic field on a stationary and sliding sessile droplet.

Magnetic particles inside a droplet have been used together with an external magnetic field. Egatz-Goméz reported the use of magnetic microparticles to drive a liquid droplet on a superhydrophobic surface.[15] More detailed results of this work were reported by García et al.[16] Pipper et al. used a permanent magnet to drive a droplet containing magnetic beads.[17] This concept was used to realize real-time polymerase chain reaction (RT-PCR) of viral ribonucleic acid (RNA) samples. Lehmann et al. used an array of planar microcoils to control droplets with magnetic beads on a planar surface.[18] Long et al. investigated the actuation of a droplet with magnetic beads using a permanent magnet.[19] An operating diagram was derived to identify the three operating regimes of the actuation concept: steady droplet transport, magnet disengagement, and particle extraction.

Due to their relatively large size, magnetic particles are not homogenously distributed in the droplet. In the presence of a strong magnetic force, the particles can even be extracted from

*To whom correspondence should be addressed. E-mail: mntnguyen@ntu.edu.sg.

(1) Chaudhury, M. K.; Whitesides, G. M. *Science* **1992**, *256*, 1539–1544.
(2) Jiao, Z. J.; Huang, X. Y.; Nguyen, N. T. *J. Micromech. Microeng.* **2008**, *18*, 045027.
(3) Pollack, M. G.; Fair, R. B.; Shenderov, A. D. *Appl. Phys. Lett.* **2000**, *77*, 1725–1727.
(4) Jiao, Z. J.; Huang, X. Y.; Nguyen, N. T. *J. Phys. A* **2008**, *41*, 355502.
(5) Daniel, S.; Chaudhury, M. K.; De Gennes, P. G. *Langmuir* **2005**, *21*, 4240–4248.
(6) Genzer, J.; Bhat, R. R. *Langmuir* **2008**, *24*, 2294–2317.
(7) Morgenthaler, S.; Zink, C.; Spencer, N. D. *Soft Matter* **2008**, *4*, 419–434.
(8) Zhang, J.; Han, Y. C. *Langmuir* **2007**, *23*, 6136–6141.
(9) Shastry, A.; Case, M. J.; Böhringer, K. F. *Langmuir* **2006**, *22*, 6161–6167.
(10) Fang, G. B.; Li, W.; Wang, X. F.; Qiao, G. J. *Langmuir* **2008**, *24*, 11651–11660.
(11) Sakai, M.; Kono, H.; Nakajima, A.; Sakai, H.; Abe, M.; Fujishima, A. *Langmuir* **2009**, *25*, 14182–14186.
(12) Sakai, M.; Kono, H.; Nakajima, A.; Sakai, H.; Abe, M.; Fujishima, A. *Langmuir* **2010**, *26*, 1493–1495.
(13) Wang, Y. L.; Bhushan, B. *Langmuir* **2010**, *26*, 4013–4017.
(14) Bormashenko, E.; Pogreb, R.; Bormashenko, Y.; Musin, A.; Stein, T. *Langmuir* **2008**, *24*, 12119–12122.
(15) Egatz-Gómez, A.; Melle, S.; Garcá, A.; Lindsay, S.; Márquez, M.; Domínguez-García, P.; Rubio, M.; Picraux, S.; Taraci, J.; Clement, T.; Yang, D.; Hayes, M.; Gust, D. *Appl. Phys. Lett.* **2006**, *89*, 034106.
(16) García, A.; Egatz-Gómez, A.; Lindsay, S.; Domińguez-Garcá, P.; Melle, S.; Marquez, M.; Rubio, M.; Picraux, S.; Yang, D.; Aella, P.; Hayes, M.; Gust, D.; Loyprasert, S.; Vazquez-Alvarez, T.; Wang, J. *J. Magn. Magn. Mater.* **2007**, *311*, 238–243.
(17) Pipper, J.; Inoue, M.; Ng, L. F. P.; Neuzil, P.; Zhang, Y.; Novak, L. *Nat. Med.* **2007**, *13*, 1259–1263.
(18) Lehmann, U.; Hadjidj, S.; Parashar, V. K.; Vandevyver, C.; Rida, A.; Gijs, M. A. M. *Sens. Actuators, B* **2006**, *117*, 457–463.
(19) Long, Z. Z.; Shetty, A. M.; Solomon, M. J.; Larson, R. G. *Lab Chip* **2009**, *9*, 1567–1575.

the droplet.[18,19] Smaller, nanoscale magnetic particles would not cause this problem, because the Brownian motion is strong enough to retain the nanoparticles. For this reason, we have used ferrofluid droplets in a number of applications.[20−22] Ferrofluid is colloidal suspension of single domain magnetic nanoparticles such as magnetite (Fe_3O_4) coated by a layer of surfactants in a carrier liquid such as water or oil. The surfactants prevent agglomeration of the particles in the presence of a magnetic field. Since the magnetic domain has the same size as the particle and does not retain the magnetic moment, ferrofluids are super paramagnetic. The small particle size causes the fluid to behave as liquid even under a strong magnetic field, where colloidal suspension of larger magentic particles such as magnetorheological fluids would behave as a solid. In our previous work, microcoils were used to control the one-dimensional[20] and two-dimensional[21] movement of a ferrofluid droplet. In these investigations, the ferrofluid droplet was suspended in another liquid phase (silicone oil); only the top view of the droplet was captured and analyzed. In other work, we used a ferrofluid droplet to push DNA samples in a polymerase chain reaction (PCR) device.[22] The ferrofluid was dragged by an external permanent magnet. Driving ferrofluid droplets using a permanent magnet proves to be a simple and reliable actuation concept for lab-on-a-chip applications. Bormashenko and Whyman reported the analysis of the shape of sessile droplets pinned to a solid substrate and exposed to the external potential.[23] This approach could be used to describe the effect of the magnetic field on a ferrofluid droplet.

In this paper, we study the magnetowetting phenomena and the sliding motion of a ferrofluid droplet on a planar surface. Permanent magnets of different sizes and strengths were used to drag the droplet along in a linear motion. The permanent magnet was attached to a translation stage to realize this motion. We first experimentally investigated the magnetowetting effect. The apparent contact angle[24] of a stationary sessile ferrofluid droplet under different magnetic field strengths was measured. Next, the dynamic contact angles and the sliding motion of the droplet were investigated. The ferrofluid droplet was first positioned and maintained in the stationary condition. The permanent magnet then approaches the ferrofluid droplet, traps it, and drags it along. This experiment allows the observation of the hysteresis of the dynamic contact angles. The evolution of the droplet shape and the change of the contact angles were captured and subsequently evaluated. Due to the stable suspension of magnetic nanoparticles, we expect only two operating regimes in this experiment: steady droplet transport and disengagement of the magnet.

Materials and Methods

Surface Preparation and Ferrofluid. The planar surface used in our experiments was prepared on a Pyrex glass wafer. We followed the recipe reported by Long et al.[19] The glass wafer was first rinsed in Piranha solution to remove any organic matter on the surface. To improve the adhesion of the Teflon coating, a solution of 1 wt % 1*H*,1*H*,2*H*,2*H*-perfluorodecyltriethoxysilane (Sigma Aldrich) was prepared. The base solution consists of isopropanol with 5 wt % water and a drop of 0.1 M HCl. The clean glass wafer was subsequently immersed in this solution for 30 s and dried at 110 °C for 15 min. Teflon solution (DuPont AF1600, 1 wt % solution in Fluorinert) was spin-coated on the fluorosilane-treated glass wafer to form a thin layer of about 200 nm Teflon. The coated glass wafer was then baked at 110 °C for 10 min, at 165 °C for 5 min, and finally at 330 °C for 15 min. The glass wafer was subsequently diced into 3 cm ×3 cm square pieces, ready for the experiments.

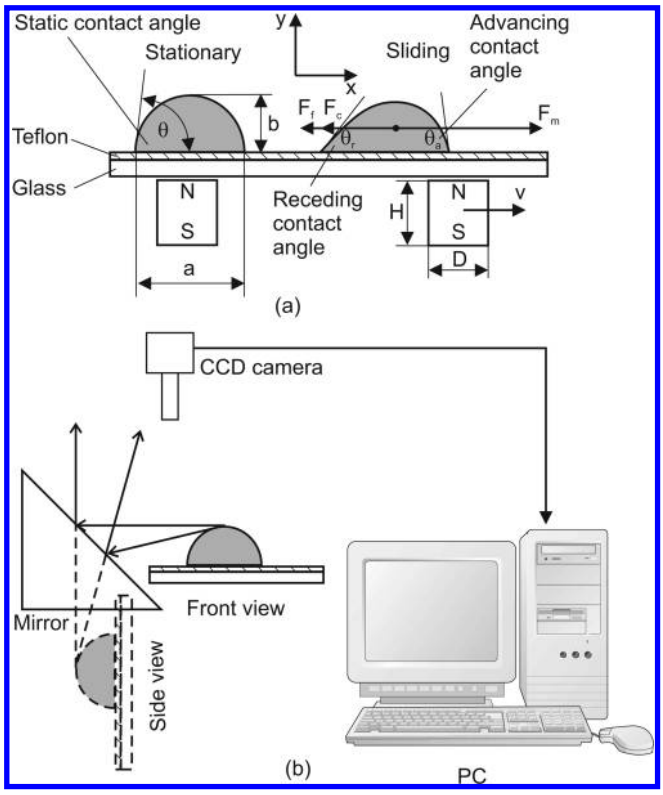

Figure 1. Experimental setup: (a) Stationary and sliding ferrofluid drop (only force components in *x*-axis are depicted). (b) Imaging system for both front view and side view of the droplet (not to scale).

Water-based ferrofluid (EMG508, Ferrotech, USA) with 1.8 vol % Fe_3O_4 nanoparticles of 10 nm diameter was used in our experiments. The magnetization of the ferrofluid is saturated at a flux density of 6 mT. Its dynamic viscosity at 27 °C is $\mu = 5$ mPa s. The density at 25 °C is $\rho = 1.07$ g/cm^3. The initial susceptibility is $\chi = 0.24$. The surface tension $\sigma = 31.66 \pm 0.05$ mN/m of the ferrofluid was measured with a commercial tensiometer (TVT-2, measurement range of 0.1 to 100 mN/m, error of ±0.01−0.05 mN/m, Lauda, Germany). With these properties, the capillary length of the ferrofluid is $l = (\sigma/\rho g)^{1/2} = 1.74$ mm.[25] For a critical Bond number $BO_{cr} = \rho g R_{cr}^2/\sigma = 1$,[25] the critical radius of the droplet would be on the order of the capillary length $R_{cr} = l$. The base diameter of the droplets in our experiments was chosen as $a < 2l = 3.48$ mm, so that the Bond number is below unity, and in the absence of the permanent magnet, the droplet can assume a spherical shape (Figure 1).

Experimental Setup. A permanent magnet was mounted on the moving stage of a syringe pump (KD Scientific, USA). The linear motion of the syringe pump is programmable; thus, the velocity of the permanent magnet can be controlled. With the help of a precision micrometer screw gauge, the top face of the permanent magnet is positioned accurately at a distance of 2 mm away from the hydrophobic surface. The Pyrex glass substrate is 0.5 mm thick. Thus, a gap of 1.5 mm between the lower surface of the glass slide and the top surface of the magnet was maintained. For calibration purpose, a plastic ruler was inserted into this gap. Three nickel-plated neodymium disk permanent magnets of different dimensions and strengths were purchased from Eclipse Magnetics (United Kingdom). We denote them here as small (N700-RB, $H = 4$ mm, $D = 2$ mm), medium

(20) Nguyen, N. T.; Ng, K. M.; Huang, X. Y. *Appl. Phys. Lett.* **2006**, *89*, 052509.
(21) Beyzavi, A.; Nguyen, N. T. *J. Micromech. Microeng.* **2010**, *20*, 015018.
(22) Sun, Y.; Nguyen, N. T.; Kwok, Y. C. *Anal. Chem.* **2008**, *80*, 6127–6130.
(23) Bormashenko, E.; Whyman, G. *Chem. Phys. Lett.* **2008**, *463*, 103–105.
(24) Bormashenko, E. *Colloids Surf., A* **2009**, *345*, 163–165.
(25) Hodges, S.; Jensen, O.; Rallison, J. *J. Fluid Mech.* **2007**, *512*, 95–131.

Table 1. Droplets with Different Sizes under Investigation

droplet type	volume (μL)	base diameter (mm)
I	0.7	1.15 ± 0.06
II	1.3	1.57 ± 0.08
III	2.3	1.97 ± 0.10
IV	3.4	2.22 ± 0.11
V	4.8	2.61 ± 0.13

Table 2. Frame Rates Used for the Different Speeds of the Magnets

speed (mm/s)	frame rate (fps)	relative error ε (%)
0.2	2	30
0.4	2	15
0.6	3	15
0.8	4	15
1.0	7	21
1.2	9	23
1.4	11	24
1.6	12	23
1.8	13	22
2.0	14	21

(N701-RB, $H = 2$ mm, $D = 3$ mm), and large (N703-RB, $H = 6$ mm, $D = 6$ mm) magnets. The height H and the diameter D of the magnet are defined in Figure 1a. The magnetic flux density of the magnets on the glass surface was measured with a commercial gaussmeter (GM04, measurement range of 0.1 to 299.9 mT, error of ± 0.1 mT, Hirst Magnetics, United Kingdom). The measured flux densities on the surface and along the magnet axis of the small, medium, and large magnets are 38 ± 0.1 mT, 64 ± 0.1 mT, and 199 ± 0.1 mT, respectively. These values are the averaged density passing through the sensor area of the gaussmeter. Although the effect of the magnetic field is three-dimensional (or two-dimensional for our axis-symmetric case) and depends on the local flux density, the measured flux density is used here as the indication of the field strength of the different magnets. The ferrofluid droplets were dispensed using a micropipet (Finnpipette, Thermo Scientific, United States). This micropipet can dispense small volumes of liquid ranging from 0.5 to 10 μL. Droplets with different volumes were investigated. Since we intend to investigate the scaling relationship based on the base diameter of the droplet with a Bond number below unity, the volumes are selected to have base diameters ranging from 1 mm to 3 mm. The droplets with different sizes are denoted as (I) to (V), Table 1.

Figure 1b shows the schematic setup of the imaging system used in the experiments reported in this paper. The images of the ferrofluid droplet were captured by a CCD camera (Pulnix, progressive scan camera, JAI Inc., Japan). The camera software (*Video Savant* 3.0, IO Industries, Ontario, Canada) can record a series of 149 image frames with a given frame rate. Since the system has a zoom objective, the size of the image frame can be adjusted accordingly. When the objective is zoomed out to its limit, the largest error caused by pixel resolution is 30 μm. In each experiment, the frame rate was adjusted to match the velocity of the magnet (Table 2). The frames are stored as images or a single movie file. To observe the side view of the droplet, a 45° mirror was placed next to the droplet. With the mirror, the camera can capture both top view and side view of the ferrofluid in a single frame. As mentioned above, a plastic ruler was placed under the glass slide to give a reference for the later evaluation of the captured images. The shape of of the ferrofluid droplet was measured automatically using a customized MATLAB program. The program converts the recorded grayscale image into a binary image for further processing. In the stationary case, the image of the droplet was evaluated to extract parameters such as contact angle, base diameter, droplet height, and radius of curvature. The data were evaluated on the basis of ten recorded frames. The error is taken as the standard deviation of the collected data. This random error is caused by the lighting condition and pixel resolution when the image is converted from grayscale format to binary format. In the case of a moving droplet, the images were processed to extract the droplet velocity and the advancing and the receding contact angles. With the known frame rate, these parameters can be plotted as functions of time. The propagation of systematic error from the measurement of displacement and the frame rate can be estimated as follows:

$$\Delta v = \left|\frac{\Delta\delta_x}{\delta_t}\right| + \left|\frac{\delta_x}{\delta_t^2}\Delta\delta_t\right| \quad (1)$$

where Δv is the error of the evaluated velocity, δ_x is the displacement of the centroid of the droplet from one frame to the next frame, δ_t is the time delay between two frames, $\Delta\delta_x$ is the systematic error caused by camera resolution, and $\Delta\delta_t$ is the systematic error caused by the timer of the frame grabber. For the worst-case estimation of the systematic error of the evaluated velocity, the displacement, the spacial error and the time error can be estimated as $\delta_x = v\delta_t$, $\Delta\delta_x = 0.03$ mm, and $\Delta\delta_t = 10^{-6}$ s. The relative systematic error of the velocity can then be calculated as $\varepsilon = \Delta v/v \times 100\%$ and listed in Table 2 for the different velocity and frame rates used in our later experiments.

The contact angles were evaluated by first extracting the droplet shape from the image. Next, a fifth-order polynomial was fitted to the droplet shape. The derivative of the fitting polynomial was calculated and used to determine the tangent and the corresponding contact angles at the two ends of the droplet. Since the coefficients of the polynomial may change in the recorded frames, it is difficult to derive a relative systematic error for the contact angles. In this paper, relative random error was used for the contact angles. The random error was evaluated on the basis of polynomial fitting lines of the data and plotted as a confidence band. The random error of the evaluated contact angle is about 4%. Because of smaller uncertainty in lighting condition and grayscale to binary conversion, a stationary droplet has a smaller random error for the contact angles. Since the capillary force is evaluated on the basis of contact angle, the random error propagates to about 25%.

Results and Discussion

Magnetowetting. We first investigated the effect of magnetic field strength on the shape and contact angle of a sessile ferrofluid droplet. This phenomenon is called magnetowetting here. Figure 2 shows the shape of droplet III under different magnetic conditions. Without a permanent magnet, the droplet has a base diameter of 1.97 ± 0.10 mm and a contact angle of $72.4 \pm 0.2°$ (Figure 2a). Under a magnetic field, the droplet is flattened and the contact angle decreases (Figure 2b,c). With the flux density of 199 ± 0.1 mT of the large magnet, the droplet takes the shape of a puddle (Figure 2d).

Figure 3 shows the measured geometric parameters of the different stationary ferrofluid droplets as a function of the flux density. In the absence of the magnet and with contact angle ranging from $70.6 \pm 0.1°$ to $73.4 \pm 0.2°$, a large ferrofluid droplet would assume a puddle form with a height of $b = 2l \sin \theta/2$ from 3.28 mm to 3.34 mm.[26] In the absence of the magnet, the height of the droplets under investigation were below 1.4 mm. Thus, the flattened puddle form shown in Figure 2 is clearly caused by the magnetic field. In general, a stronger magnetic field would pull down and laterally stretch the ferrofluid droplet, increasing its base diameter, decreasing its height and decreasing its apparent contact angle (Figure 3). While the base diameter of the ferrofluid

(26) Berthier, J.; Silberzan, P. *Microfluidics and Biotechnology*; Artech House, 2009.

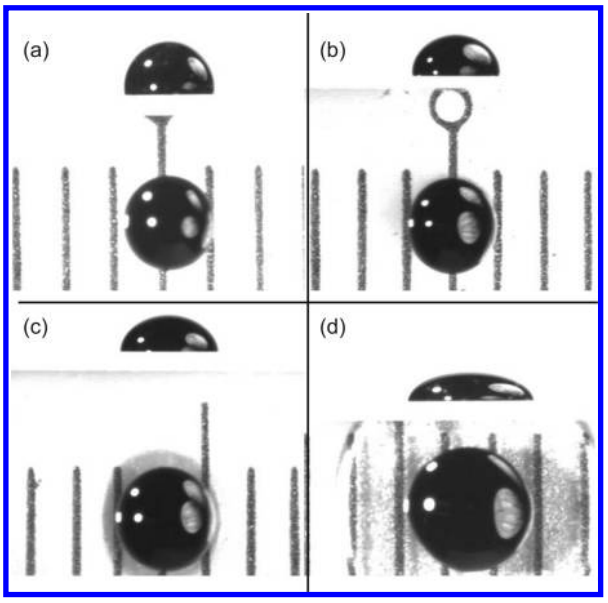

Figure 2. Sessile ferrofluid droplet (III, $V = 2.3\ \mu$L) under different magnetic field strengths: (a) no magnet; (b) small magnet, $B = 38 \pm 0.1$ mT; (c) medium magnet, $B = 64 \pm 0.1$ mT; (d) large magnet, $B = 199 \pm 0.1$ mT.

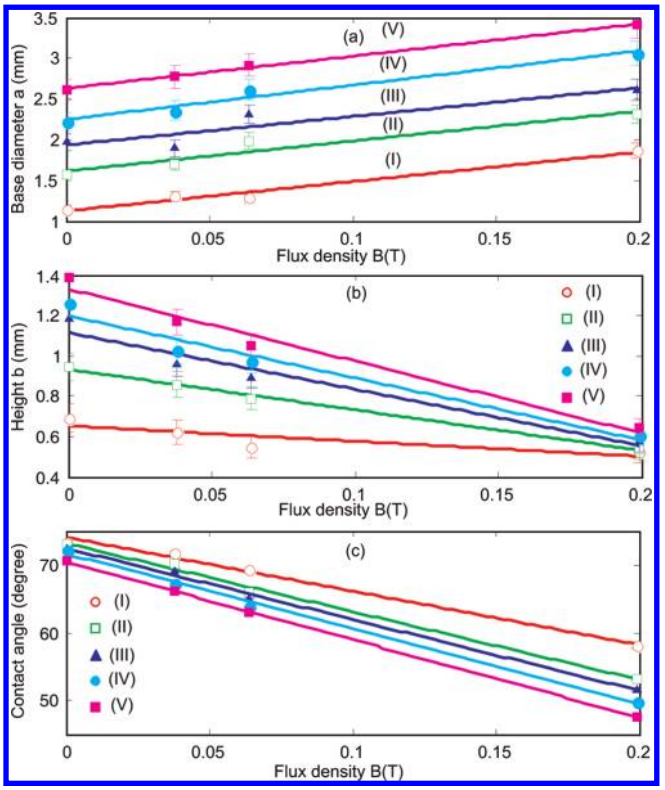

Figure 3. Magnetowetting effect of stationary ferrofluid droplets of different sizes (the lines are second-order fitting curves): (a) Base diameter. (b) Droplet height. (c) Apparent contact angle .

droplet increases almost linearly with the flux density (Figure 3a), its height tends to reach an asymptotic value of about 0.6 mm (Figure 3b). The observed behavior is similar to that of a large droplet with a large Bond number. In our case, the magnetic force is a significant body force which can be 1 or 2 orders of magnitude higher than gravitational force. Values extracted from the sliding experiments support this hypothesis.

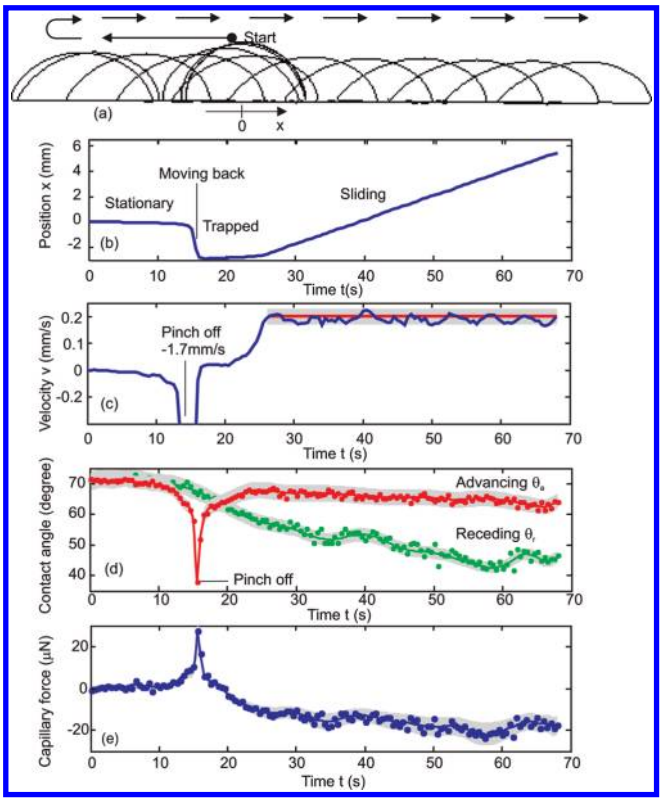

Figure 4. Sliding of a sessile ferrofluid droplet in the presence of a moving permanent magnet ($H = 2$ mm, $D = 3$ mm, $B = 64$ mT, $v = 0.2$ mm/s, and $a \approx 2.22$ mm): (a) Evolution of the tracked droplet (every 10 frames). (b) Displacement of the droplet centroid versus time. (c) Velocity of the droplet versus time. The constant velocity of 0.2 mm/s is plotted as the redline with a confidence band of ±30%. (d) Contact angles versus time. The confidence interval is ±4%. (e) Capillary force versus p time. The confidence interval is ±25%.

Sliding of a Sessile Ferrofluid Droplet. *Droplet Kinematics*. In our experiments, three parameters were varied: three different magnets (small, medium, and large), five different base diameters (Table 1), and ten different magnet velocities ranging from 0.2 to 2 mm/s. Two basic operating regimes were observed: sliding (Figure 4) and disengagement (Figure 5). The following analysis estimates the order of magnitude of the different forces involved in the sliding process. These numbers will be used to estimate the scaling factors of the operating map discussed in the next section.

If the magnet is slow enough and the magnetic force is large enough (strong magnet or large droplet), the ferrofluid droplet can slide with the same velocity as the magnet. Figure 4 shows the typical behavior of a ferrofluid droplet in the sliding regime. Without the magnet, the stationary droplet has a contact angle of 72°. Figure 4a shows the time-evolving image of the ferrofluid droplet IV with an initial base diameter of 2.22 mm as the medium magnet moves in from the right at a velocity of 0.2 mm/s. The approaching magnet pulls the droplet to the right. The droplet deforms so that the right contact angle (the later advancing contact angle, red line in Figure 4d) decreases significantly. Since the droplet is still stationary, only the capillary force resists the magnetic force. At the pinching moment, the solid/liquid/gas contact line is displaced and the right and left contact angles drop to $\theta_a = 38°$ and $\theta_r = 67°$, respectively. The capillary force and the magnetic force can be estimated for this moment as $F_{mag} = F_{cap} = a\sigma(\cos\theta_a - \cos\theta_r) \approx 28\ \mu$N.[26] Figure 4e shows the

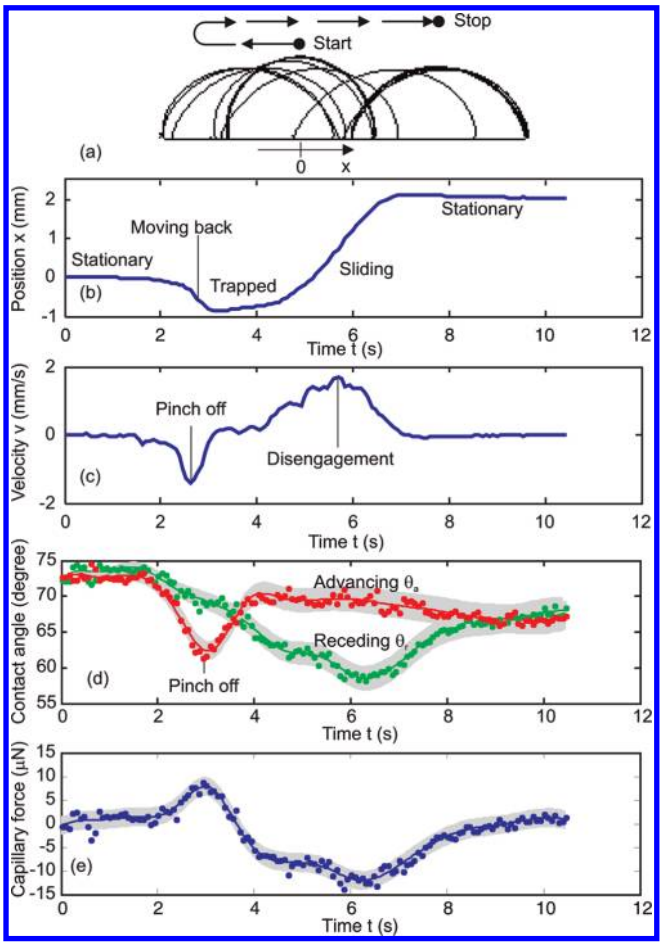

Figure 5. Disengagement of a sessile ferrofluid droplet in the presence of a fast moving permanent magnet (H = 2 mm, D = 3 mm, $a \approx 2.22$ mm, 64 mT, 1.8 mm/s): (a) Evolution of the tracked droplet (every 10 image frames). (b) Displacement of the droplet centroid versus time. (c) Velocity of the droplet versus time. (d) Contact angles versus time. The confidence interval is ±4%. (e) Capillary force versus time. The confidence interval is ±25%.

capillary force as a function of time. To appreciate the magnitude of the magnetic force, the weight of the droplet calculated with the given volume of V = 3.4 μL and density of ρ = 1.07 g/cm^3 is 3.64 μN. From the pinching moment, the droplet accelerates to 1.7 mm/s. After being trapped on the magnet, the droplet continues to deform and accelerates to the steady velocity of the magnet (Figure 4b). In this process, the relative distance between the magnet and the droplet is adjusted to reach an equilibrium between capillary force, friction force, and magnetic force. The evaluated velocity shows a wavy characteristics, which is caused by the stepper motor driving the linear stage. The advancing contact angle then reaches a steady-state value of approximately 64°, while the receding contact angle approaches a value of approximately 46°. The capillary force in the steady-state sliding motion remains constant at a value of $F_{cap} \approx 18$ μN (Figure 4e).

With the same condition as the previous experiment (Figure 4), the droplet cannot move if the magnet velocity is higher than 1.6 m/s. Figure 5 shows the behavior of the droplet at v = 1.8 m/s. Similar to the previous case, the droplet was pinched off by the approaching magnet. With θ_a = 61° and θ_r = 69°, the magnetic force at the pinching moment is approximately $F_{mag} = F_{cap} \approx$ 9 μN (Figure 5e). This force is smaller than in the previous case because of the higher approaching velocity, and the exact pinching moment cannot be captured. The droplet first accelerates to reach the steady velocity of the magnet, where the disengagement occurs because the velocity subsequently drops. At this disengagement moment, the contact angles were measured as θ_a = 69° and θ_r = 60°. The corresponding capillary force is $F_{cap} \approx 10$ μN. Subsequently, the receding contact angle reaches a minimum value of θ_r = 58°, where the advancing contact angle is θ_a = 70°. The corresponding capillary force at this moment is $F_{cap} \approx 13$ μN. After becoming stationary again, the contact angle on both sides of the droplet reaches 67°, dropping from the initial 73°.

Next, we investigated the dependence of the droplet kinematics on the magnetic strength, base diameter, and velocity of the moving magnet. Figure 6a compares the behavior of the smallest droplet I (Table 1) affected by three different magnets moving at the same velocity of 0.2 mm/s. The small magnet can pinch off the droplet and pull it back. However, the magnetic force is not large enough to return the droplet to its original position. As the small magnet moves away, the droplet is positioned 100 μm to the left of the initial position. The contact angle reduces from the initial value of 73° to 68°. The same behavior was observed with the medium magnet. However, the magnet is strong enough to drag the droplet forward, so that after the disengagement, the droplet is positioned 200 μm to the right of the initial position. The large magnet is strong enough to drag the droplet along. The behavior is similar to that described in Figure 4. The strength of the magnetic force is correlated well with the trapping position.

Figure 6b shows the kinematic behavior of droplets with different sizes. The droplets are dragged by the medium magnet at 0.2 mm/s. Similar to the case for different magnets, the magnetic force depends on the size of the droplet. Small droplets have a weak magnetic force and consequently cannot slide along with the magnet. Besides the magnetic force, the base diameter also affects the friction force, which in turns affects the behavior of the droplet displacement. With an optimal size (droplet II), the magnetic force is balanced by the friction force minimizing the displacement of the droplet. Figure 6b shows that droplet II has both the smallest displacement and trapping distance. As discussed later by the scaling analysis, the magnetic force scales with the third order of the base diameter and the friction force with the second order of the base diameter. Large droplets make the magnetic force strong enough to overcome initial friction and to slide into motion. In the case of droplet IV, the magnetic force just reaches the threshold causing the sliding velocity to fluctuate due to the readjustment of the relative distance between the droplet and the magnet. Droplet V is large enough so that the distance and consequently the magnetic force are steady during the sliding motion.

Figure 6c shows the behavior of droplet II dragged by the medium magnet at different velocities. The kinematic behavior clearly shows the effect of the friction force, which is proportional to the velocity of the droplet. At 0.2 and 0.4 mm/s, the droplet is still able to follow the magnet. At velocities higher than 0.6 mm/s, the friction force is so large that disengagement occurs. The following scaling analysis discusses the relationship among the velocity, the base diameter, and the sliding regimes in more details.

Scaling Analysis and Operating Map. The kinematic behavior depicted in Figure 6 indicates the three parameters determining the operating regime of a sliding ferrofluid droplet: the magnetic field strength, the size of the droplet represented by its base diameter, and the velocity of the magnet. Since the magnetic field strength is adjusted in the droplet/surface/magnet system by the distance between the magnet and the droplet, the two key parameters for developing the scaling relationships and the

 DOI: 10.1021/la101474e E

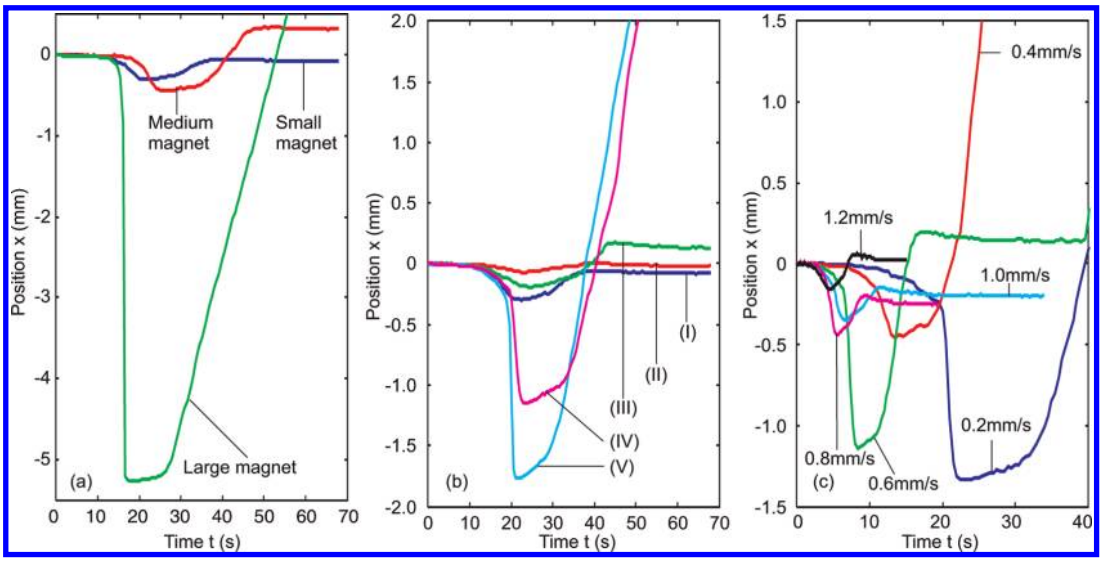

Figure 6. Dependence of droplet kinematics on different parameters: (a) Magnetic strength (droplet I, magnet velocity of 0.2 mm/s). (b) Base diameter of droplet (medium magnet, magnet velocity of 0.2 mm/s). (c) Velocity of the magnet (medium magnet, droplet II).

operating map for the sliding ferrofluid droplet are the base diameter a and the magnet velocity v.

As shown in Figure 1a, the force balance in the x-axis of a sliding ferrofluid droplet is

$$F_{mag} = F_{fric} + F_{cap} \tag{2}$$

where F_{mag} is the driving magnetic force, F_{fric} is the friction force, and F_{cap} is the capillary force caused by the difference between advancing and receding contact angles.

The magnetic force is determined by

$$F_{mag} = \frac{V\chi}{\mu_0}\mathbf{B}\nabla\mathbf{B} = \alpha a^3 \tag{3}$$

where $V \propto a^3$ is the volume of the droplet, χ is the magnetic susceptibility of the ferrofluid, μ_0 is the permittivity of free space, and $\mathbf{B}$ is the magnetic field applied on the droplet. With a fixed relative position between the droplet and the magnet, factor α represents the strength of the magnetic field. The scaling relationship of the magnetic force is $F \propto a^3$.

The friction force acting against the sliding motion of the droplet can be estimated as

$$F_{fric} = K_f A\mu v = \beta a^2 v \tag{4}$$

where K_f is the friction factor, $A = \pi a^2/4$ is the contact area, μ is the viscosity of the ferrofluid, and v is the velocity of the magnet and the droplet. The above relationship considers the flattened shape of the droplet due to the strong magnetic pull, where the factor K_f is assumed to be constant. The scaling relationship of the friction force is $F_{fric} \propto a^2$. The factor β represents the friction between the droplet and the solid surface.

The capillary force acting against the sliding motion is

$$F_{cap} = a\sigma(\cos\theta_r - \cos\theta_a) = \gamma a \tag{5}$$

where σ is the surface tension of the ferrofluid. Since the advancing and receding contact angles θ_a, θ_r remains constant in the steady-state sliding condition, The factor γ represents the strength of capillarity. The scaling relationship of the capillary force is $F_{fric} \propto a$.

The droplet can slide if a critical velocity v_{cr} is reached. The force balance has the form

$$\alpha a^3 = \beta a^2 v_{cr} + \gamma a \tag{6}$$

Rearranging the above equation leads to the scaling relationship between the critical velocity and the base diameter of the droplet

$$v_{cr} = \frac{\alpha}{\beta}a - \frac{\gamma}{\beta}\frac{1}{a} \tag{7}$$

Figure 7a depicts the two terms forming the curve of the critical velocity on the velocity/base diameter operating map. The shaded area to the right of the curve represents the sliding regime. In this region, the magnetic force is large enough to overcome the friction and to drag the droplet along. A low velocity and a large droplet would make sliding possible. Therefore, the sliding region occupies the lower right-hand corner of the operating map. Figure 7b shows the operating map observed in our experiments. The red, green, and blue-shaded areas are the sliding regions of the small magnet, medium magnet, and large magnet, respectively.

The parameters α, β, and γ from the scaling analysis were used to fit the experimental data. To start with, we used data of the medium magnet and droplet IV (Figure 4) due to the relatively low noise of the data of the capillary force. The maximum capillary force of the pinch-off moment of 28 μN is used to estimate the magnetic force. From eq 3 and $a = 2.22$ mm, the scaling factor for the magnetic force is determined as $\alpha \approx 3\,\mu\text{N/mm}^3$. From eq 5 and a capillary force during the sliding motion of $F_{cap} \approx 18$ μN, the scaling factor for the capillary force is determined as $\gamma = 8\,\mu$N/mm. Since there is no further information for the estimation of the friction force, the values of α and β were used to find $\beta = 2\,\mu\text{N s/mm}^3$ so that the curve of eq 7 can fit the experimental data of the medium magnet, Figure 7b. Subsequently, the values of $\gamma = 8\,\mu$N/mm and $\beta = 2\,\mu\text{Ns/mm}^3$ and eq 7 were used to find $\alpha \approx 1.5\,\mu\text{N/mm}^3$ and $\alpha \approx 8\,\mu\text{N/mm}^3$ that can fit the data of the small and the large magnet, respectively.

The above scaling analysis and fitting scaling factors only qualitatively explain the interactions among the forces involved in the sliding motion. In fact, only the magnitude of the capillary force can be extracted from the measurement. The magnetic force at the pinch-off moment is not necessarily the same as the

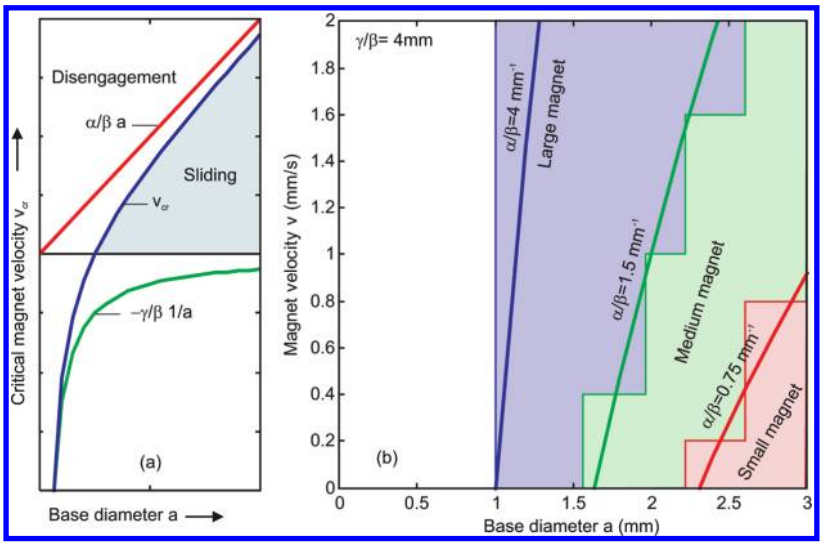

Figure 7. Operating map of a sliding ferrofluid droplet: (a) Scaling law for the critical velocity. (b) Operating map of the ferrofluid droplets in our experiments ($\beta \approx 2\ \mu$N s/mm^3, $\gamma \approx 8\ \mu N$/mm). The red-shaded area is the sliding regime with the small magnet ($\alpha \approx 1.5\ \mu$N/mm^3) The green-shaded area is the sliding region of the medium magnet ($\alpha \approx 3\ \mu$N/mm^3). The sliding region of the large magnet is shaded in blue ($\alpha \approx 8\ \mu$N/mm^3).

magnetic force during the sliding motion, because the relative distance between the droplet and the magnet is changed with the speed of the magnet. Depending on the speed and the size of the magnet, the relative distance and the magnetic force can vary. The friction force depends on the gravitational force and also the *y*-component of the magnetic force. Since the *y*-component of the magnetic force can be 1 or 2 orders of magnitude larger than the weight of the droplet, the friction force is also dominated by the magnetic force, which in turn varies as mentioned above.

Conclusions

This study experimentally investigates the effect of magnetowetting and the sliding motion of a sessile ferrofluid droplet. The results show that the shape of a sessile ferrofluid droplet is deformed in the presence of a magnetic field. The deformation depends on the local magnetic field. Using permanent magnets, we are able to observe the basic features of magnetowetting phenomenon. A higher flux density leads to a larger base diameter and a smaller height. More importantly, a higher flux density reduces the contact angle at the solid/liquid/gas contact line. This paper also investigates the kinematic behavior of the droplet dragged by the permanent magnet at a constant velocity. If the magnetic force is large enough to overcome the resistance of the friction force and the capillary force, the droplet can slide along with the same linear velocity as the magnet. This paper reports the detailed kinematic behavior of the droplet as well as the change of its contact angles. Contact angle hysteresis was observed from the droplet after being pinched off from its initial position and resuming the stationary condition. Scaling analysis was developed to describe the operation regions of the sliding ferrofluid droplets. On a velocity-versus-base-diameter operating map, the sliding region occupies the lower right-hand corner. The critical velocities derived from the scaling analysis and parameters fitted to experimental data describe this map well. A more detailed analytical model or a numerical model are needed to explain and to appreciate the phenomena observed in the experiments. Results reported here on magnetowetting effect and magnetic manipulation of ferrofluid droplets in particular or magnetic droplets in general would have potential impacts on droplet-based microfluidics, interface control of liquid lenses, and possibly e-paper technology.